A Review of the Path Integral Time Domain Method

Jeffrey A. Miller, Ph.D.

Abstract

The path integral time domain method (PITD) is a relatively new numerical technique for electromagnetic scattering, propagation, and transmission line analysis. The underlying theory and numerical technique are demonstrated and several one-dimensional problems illustrate the interesting properties of the method

Introduction

The path integral time-domain method as introduced by Nevels[1] has several intriguing properties. These include the collocation of the electric and magnetic fields, the absence of numerical dispersion, and the spatial domain sampling at the Nyquist limit. This paper will review the theory and numerical procedure of the path integral time domain method. One-dimensional examples illustrate the most practical applications of the method at its current state of development.

Maxwell's Equations

Maxwell's time dependent equations for a source free region are given by

$$\nabla \times \mathbf{H} = \sigma \cdot \mathbf{E} + \varepsilon \cdot \frac{\partial \mathbf{E}}{\partial t} \tag{1}$$

$$\nabla \times \mathbf{E} = -\rho \cdot \mathbf{H} - \mu \cdot \frac{\partial \mathbf{H}}{\partial t} \tag{2}$$

where σ and ρ are the electric and magnetic(fictitious) conductivities, and $\mathbf{E}$ and $\mathbf{H}$ are the electric and magnetic field intensities. Throughout this paper vector quantities are denoted by bold face type. The permittivity ε and permeability μ of the medium are real numbers that are time independent. Combining the two curl equations into a single vector equation leads to

$$\frac{\partial \mathbf{F}}{\partial t} = \bar{\mathbf{S}} \cdot \mathbf{F} \tag{3}$$

by isolating the time derivatives on the left hand side and creating a new vector

$$\mathbf{F}^{\mathrm{T}} = \begin{bmatrix} E_x & E_y & E_z & H_x & H_y & H_z \end{bmatrix} \text{ and the matrix}$$

$$\bar{\mathbf{S}} = \begin{bmatrix} -\sigma/\varepsilon & \varepsilon^{-1} \cdot \nabla \times \\ -\mu^{-1} \cdot \nabla \times & -\rho/\mu \end{bmatrix}. \tag{4}$$

The Propagator

The propagator plays a significant role in the PITD method. As will be shown, the propagator is the mechanism by which fields are advanced in time and propagated in space. Barton [2] states that a propagator $\bar{\mathbf{K}}$ is found by solving equation (3), which is a vector hyperbolic equation, substituting $\bar{\mathbf{K}}$ for $\mathbf{F}$ as in equation (5) and adding the initial condition shown in equation (6).

$$\frac{\partial \bar{\mathbf{K}}}{\partial t} = \bar{\mathbf{S}} \cdot \bar{\mathbf{K}} \tag{5}$$

$$\lim_{t \to t'} \bar{\mathbf{K}}(\mathbf{r}, \mathbf{r}'; t, t') = \bar{\mathbf{I}} \delta(\mathbf{r} - \mathbf{r}') \tag{6}$$

In equation (6), $\bar{\mathbf{I}}$ is the identity matrix, $\delta(\mathbf{r} - \mathbf{r}')$ is the Dirac delta function, t, t' are the current and initial times, and the vectors $\mathbf{r}, \mathbf{r}'$ represent the current and initial spatial locations respectively. In Cartesian coordinates, $\mathbf{r} = x\hat{\mathbf{x}} + y\hat{\mathbf{y}} + z\hat{\mathbf{z}}$ where unit vectors are denoted by bold face type with hats. The initial vector is likewise $\mathbf{r}' = x'\hat{\mathbf{x}} + y'\hat{\mathbf{y}} + z'\hat{\mathbf{z}}$. By straightforward substitution a solution to (5) is

$$\bar{\mathbf{K}} = \mathrm{e}^{\bar{\mathbf{S}} t} \, \bar{\mathbf{K}}_{\mathbf{0}} . \tag{7}$$

Using the initial condition (6) with (7), leads to

$$\bar{\mathbf{K}}_{\mathbf{0}} = \mathrm{e}^{-\bar{\mathbf{S}} t'} \, \bar{\mathbf{I}} \delta(\mathbf{r} - \mathbf{r}') . \tag{8}$$

Substituting (8) into (7) gives the final form of the propagator as

$$\bar{\mathbf{K}} = e^{\bar{\mathbf{S}}(t)} e^{\bar{\mathbf{S}}(-t')} \bar{\mathbf{I}} \delta(\mathbf{r} - \mathbf{r}') = e^{\bar{\mathbf{S}}(\tau)} \bar{\mathbf{I}} \delta(\mathbf{r} - \mathbf{r}') . \tag{9}$$

Finally, the delta function in (9) is replaced with its spatial inverse Fourier transform representation

$$\delta(\mathbf{r} - \mathbf{r}') = \int_{-\infty}^{\infty} \mathrm{e}^{j 2\pi \mathbf{k} \cdot (\mathbf{r} - \mathbf{r}')} d\mathbf{k} \tag{10}$$

giving

$$\bar{\mathbf{K}}(\mathbf{r}, \mathbf{r}'; \tau) = \mathrm{e}^{\bar{\mathbf{S}} \tau} \, \bar{\mathbf{I}} \int_{-\infty}^{\infty} \mathrm{e}^{j 2\pi \mathbf{k} \cdot (\mathbf{r} - \mathbf{r}')} d\mathbf{k} . \tag{11}$$

Equation (11) doesn't appear to simplify the expression for the propagator but with a little linear algebra, a new propagator matrix that is more beneficial is obtained. The $\bar{\mathbf{S}}$ matrix for a simple inhomogeneous, isotropic medium in three-dimensional Cartesian coordinates is

$$\bar{\mathbf{S}} = \begin{bmatrix} -\sigma/\varepsilon & 0 & 0 & 0 & -(1/\varepsilon)\partial_z & (1/\varepsilon)\partial_y \\ 0 & -\sigma/\varepsilon & 0 & (1/\varepsilon)\partial_z & 0 & -(1/\varepsilon)\partial_x \\ 0 & 0 & -\sigma/\varepsilon & -(1/\varepsilon)\partial_y & (1/\varepsilon)\partial_x & 0 \\ 0 & (1/\mu)\partial_z & -(1/\mu)\partial_y & -\rho/\mu & 0 & 0 \\ -(1/\mu)\partial_z & 0 & (1/\mu)\partial_x & 0 & -\rho/\mu & 0 \\ (1/\mu)\partial_y & -(1/\mu)\partial_x & 0 & 0 & 0 & -\rho/\mu \end{bmatrix} . \tag{12}$$

In (12), ∂_i indicates a partial derivative with respect to the subscript. Notice that the matrix $\bar{\mathbf{S}}$ is an operator matrix that operates on $\mathbf{r}$ but not on $\mathbf{k}$. Therefore, move the exponential with the matrix $\bar{\mathbf{S}}$ under the integral sign where it operates on $\exp(j 2\pi \mathbf{k} \cdot \mathbf{r})$ with the result that the partial derivatives are replaced with the components of $\mathbf{k}$ as seen in (13).

$$\partial_x \to j2\pi k_x \quad \partial_y \to j2\pi k_y \quad \partial_z \to j2\pi k_z \tag{13}$$

The new form of $\bar{\mathbf{S}}(\mathbf{r},\mathbf{k})$ is

$$\bar{\mathbf{S}}(\mathbf{r},\mathbf{k}) = \begin{bmatrix} -\sigma/\varepsilon & 0 & 0 & 0 & \dfrac{-j2\pi k_z}{\varepsilon} & \dfrac{j2\pi k_y}{\varepsilon} \\ 0 & -\sigma/\varepsilon & 0 & \dfrac{j2\pi k_z}{\varepsilon} & 0 & \dfrac{-j2\pi k_x}{\varepsilon} \\ 0 & 0 & -\sigma/\varepsilon & \dfrac{-j2\pi k_y}{\varepsilon} & \dfrac{j2\pi k_x}{\varepsilon} & 0 \\ 0 & \dfrac{j2\pi k_z}{\mu} & \dfrac{-j2\pi k_y}{\mu} & -\rho/\mu & 0 & 0 \\ \dfrac{-j2\pi k_z}{\mu} & 0 & \dfrac{j2\pi k_x}{\mu} & 0 & -\rho/\mu & 0 \\ \dfrac{j2\pi k_y}{\mu} & \dfrac{-j2\pi k_x}{\mu} & 0 & 0 & 0 & -\rho/\mu \end{bmatrix}. \quad (14)$$

Matrix $\bar{\mathbf{S}}(\mathbf{r},\mathbf{k})$ is shown as a function of $\mathbf{r}$ as the material parameters $(\mu,\varepsilon,\sigma,\rho)$ vary with position. The propagator becomes

$$\bar{\mathbf{K}}(\mathbf{r},\mathbf{r}';\tau) = \int_{-\infty}^{\infty} \mathrm{e}^{\bar{\mathbf{S}}(\mathbf{r},\mathbf{k})\tau}\, \mathrm{e}^{j2\pi\mathbf{k}\cdot(\mathbf{r}-\mathbf{r}')} d\mathbf{k}\,. \quad (15)$$

Readers familiar with state space techniques will realize that the exponential of $\bar{\mathbf{S}}(\mathbf{r},\mathbf{k})\tau$ is changed into a state transition matrix (fundamental matrix in many mathematical texts) by several techniques (DeRusso, *et al.* [3] and Wiberg [4]). The eigenvalue approach is discussed. The eigenvalues and eigenvectors of $\bar{\mathbf{S}}(\mathbf{r},\mathbf{k})$ are sought. A modal matrix $\bar{\mathbf{M}}$ is a column-oriented compilation of the eigenvectors. The state transition matrix $\bar{\mathbf{A}}$ is

$$\bar{\mathbf{A}} = \bar{\mathbf{M}}\,\mathbf{P}(\lambda_i\tau)\,\bar{\mathbf{M}}^{-1} \quad (16)$$

where $\mathbf{P}(\lambda_i\tau)$ is a diagonal matrix with the eigenvalues of $\bar{\mathbf{S}}(\mathbf{r},\mathbf{k})$ multiplied by τ. The eigenvalues and eigenvectors are aligned such that the eigenvector in the first column of the modal matrix corresponds to the eigenvalue located in the first diagonal element. The second column of the modal matrix is another eigenvector and its associated eigenvalue is the second term in the diagonal matrix. This pattern is repeated for each eigenvalue-eigenvector pair. The inverse of the modal matrix $\bar{\mathbf{M}}^{-1}$ is the last term on the right hand side of (16). The propagator takes the simple form

$$\bar{\mathbf{K}}(\mathbf{r},\mathbf{r}';\tau) = \int_{-\infty}^{\infty} \bar{\mathbf{A}}\, \mathrm{e}^{j2\pi\mathbf{k}\cdot(\mathbf{r}-\mathbf{r}')} d\mathbf{k} \quad (17)$$

where, for example, in a lossless $(\sigma \to 0,\, \rho \to 0)$ region $\bar{\mathbf{A}}$ is

$$\overline{\mathbf{A}} = \begin{bmatrix} a_{11} & a_{12} & a_{13} & a_{14} & a_{15} & a_{16} \\ a_{21} & a_{22} & a_{23} & a_{24} & a_{25} & a_{26} \\ a_{31} & a_{32} & a_{33} & a_{34} & a_{35} & a_{36} \\ a_{41} & a_{42} & a_{43} & a_{44} & a_{45} & a_{46} \\ a_{51} & a_{52} & a_{53} & a_{54} & a_{55} & a_{56} \\ a_{61} & a_{62} & a_{63} & a_{64} & a_{65} & a_{66} \end{bmatrix} \tag{18}$$

with

$$\begin{aligned}
a_{11} &= a_{44} = \left[k_x^{\,2} + \left(k_y^{\,2} + k_z^{\,2} \right) \cos(u) \right] \Big/ k^2 \\
a_{12} &= a_{21} = a_{45} = a_{54} = k_x k_y \left(1 - \cos(u) \right) \Big/ k^2 \\
a_{13} &= a_{31} = a_{46} = a_{64} = k_x k_z \left(1 - \cos(u) \right) \Big/ k^2 \\
a_{14} &= a_{25} = a_{36} = a_{41} = a_{52} = a_{63} = 0 \\
a_{15} &= -a_{24} = -j\eta k_z \sin(u) \Big/ k \\
a_{16} &= -a_{34} = j\eta k_y \sin(u) \Big/ k \\
a_{22} &= a_{55} = \left[k_y^{\,2} + \left(k_x^{\,2} + k_z^{\,2} \right) \cos(u) \right] \Big/ k^2 \\
a_{23} &= a_{32} = a_{56} = a_{65} = k_y k_z \left(1 - \cos(u) \right) \Big/ k^2 \\
a_{26} &= -a_{35} = -j\eta k_x \sin(u) \Big/ k \\
a_{33} &= a_{66} = \left[k_z^{\,2} + \left(k_x^{\,2} + k_y^{\,2} \right) \cos(u) \right] \Big/ k^2 \\
a_{42} &= -a_{51} = jk_z \sin(u) \Big/ \eta k \\
a_{43} &= -a_{61} = -jk_y \sin(u) \Big/ \eta k \\
a_{53} &= -a_{62} = jk_x \sin(u) \Big/ \eta k \qquad ,
\end{aligned} \tag{19}$$

$$u = 2\pi k v_p \tau \text{ and } k^2 = k_x^{\,2} + k_y^{\,2} + k_z^{\,2} .$$

The Path Integral for Electromagnetic Scattering

Barton [2] writes that once the propagator is known an initial field distribution $\mathbf{F}_0$ is propagated a single time step by

$$\mathbf{F}(\mathbf{r},t) = \int_{-\infty}^{\infty} \overline{\mathbf{K}}(\mathbf{r},\mathbf{r}';\tau)\mathbf{F}_0(\mathbf{r}',t')\,d\mathbf{r}' . \tag{20}$$

Putting equation (17) into equation (20) gives

$$\mathbf{F}(\mathbf{r},t) = \int_{-\infty}^{\infty} \int_{-\infty}^{\infty} \overline{\mathbf{A}}\, \mathrm{e}^{j2\pi\mathbf{k}\cdot(\mathbf{r}-\mathbf{r}')} d\mathbf{k}\, \mathbf{F}_0(\mathbf{r}',t')\,d\mathbf{r}' . \tag{21}$$

Since $\mathbf{F}_0(\mathbf{r}',t')$ is not a function of $\mathbf{k}$, $\overline{\mathbf{A}}$ and $\exp(j2\pi\mathbf{k}\cdot\mathbf{r})$ are not functions of the initial spatial vector $\mathbf{r}'$, equation (21) is after reversing the order of integration

$$\mathbf{F}(\mathbf{r},t) = \int_{-\infty}^{\infty} \int_{-\infty}^{\infty} \bar{\mathbf{A}}\, \mathbf{F}_0(\mathbf{r}',t') \mathrm{e}^{j2\pi \mathbf{k}\cdot\mathbf{r}} \mathrm{e}^{-j2\pi \mathbf{k}\cdot\mathbf{r}'} d\mathbf{r}' d\mathbf{k}. \tag{22}$$

Equation (22) reveals significant insight into the operation of this method. Moving $\bar{\mathbf{A}}$ and $\exp(j2\pi\mathbf{k}\cdot\mathbf{r})$ outside of the internal integral

$$\mathbf{F}(\mathbf{r},t) = \int_{-\infty}^{\infty} \bar{\mathbf{A}} \left\{ \int_{-\infty}^{\infty} \mathbf{F}_0(\mathbf{r}',t') \mathrm{e}^{-j2\pi \mathbf{k}\cdot\mathbf{r}'} d\mathbf{r}' \right\} \mathrm{e}^{j2\pi \mathbf{k}\cdot\mathbf{r}} d\mathbf{k}. \tag{23}$$

Equation (23) is a remarkable and exciting equation! The initial field distribution is Fourier transformed into the spectral domain, multiplied by the transition matrix and inverse Fourier transformed back to the time-space domain. This current spatial distribution then becomes the initial field for the next time step. Assuming that τ is some small incremental element of time and $t = N\tau + t_0$, a time evolving picture of the electromagnetic field distribution is obtained by repeated application of equation (23)

$$\mathbf{F}(\mathbf{r},t) = \mathscr{F}^{-1}\left\{ \bar{\mathbf{A}}_N \mathscr{F}\left\{ \mathscr{F}^{-1}\left\{ \bar{\mathbf{A}}_{N-1} \cdots \mathscr{F}\left\{ \mathscr{F}^{-1}\left\{ \bar{\mathbf{A}}_1 \mathscr{F}\left\{ \mathbf{F}_0(\mathbf{r}',t_0) \right\} \right\} \right\} \cdots \right\} \right\} \right\}. \tag{24}$$

Equation (24) is a symbolic representation of the path integral for electromagnetic scattering. A careful observer might mention that (24) has successive operations of inverse and forward Fourier transforms that allows their removal. For a strictly homogeneous region, which is not very interesting in a practical sense, (24) reduces to a single forward transform of the initial field distribution, the transition matrix is then applied N times, and a single inverse Fourier transform gives the final field distribution

$$\mathbf{F}(\mathbf{r},t) = \mathscr{F}^{-1}\left\{ \bar{\mathbf{A}}_N \left\{ \bar{\mathbf{A}}_{N-1} \cdots \left\{ \bar{\mathbf{A}}_1 \mathscr{F}\left\{ \mathbf{F}_0(\mathbf{r}',t_0) \right\} \right\} \cdots \right\} \right\}. \tag{25}$$

In a general inhomogeneous space, the above statement and equation is *not true* because the transition matrix is a function of $\mathbf{r}$.

Numerical Method

Examining a single time step (23), it is apparent that Fourier transforms are an important aspect of this method. Ziemer, *et al.* [5] state that a bandwidth limited signal having no frequency components above a certain frequency f_h is completely specified by samples taken at a uniform rate greater than $2f_h$ which is known as the Nyquist limit. As a minimum, a numerical space is sampled at twice the rate of the highest frequency of interest. For example, if the highest frequency of interest is 3 GHz, then the minimum spatial sampling is 0.05 meters between samples assuming the phase velocity in the medium is 3×10^8 m/s. Since the continuous space is now a discretely sampled numerical space, the Fourier transforms are performed by discrete equivalents (Press, *et al.* [6])

$$X\left(n_i \triangle \mathbf{k}\right) = \sum_{m_i=0}^{N_i-1} x\left(m_i \triangle \mathbf{r}\right) \mathrm{e}^{-j2\pi n_i m_i / N_i} \tag{26}$$

$$x\left(m_i \triangle \mathbf{r}\right) = \frac{1}{N_i} \sum_{n_i=0}^{N_i-1} X\left(n_i \triangle \mathbf{k}\right) \mathrm{e}^{j2\pi n_i m_i / N_i} \tag{27}$$

where the i subscript indicates multidimensional capacity. For example, (26) for a two dimensional transform has a double summation. N_i is the total number of spatial samples in the i^{th} dimension. The spatial discretization yields a spectral domain with

$$\triangle k_i = \frac{1}{N_i \triangle r_i} \tag{28}$$

where $\triangle r_i$ represents one of the spatial elements $\triangle x, \triangle y$, or $\triangle z$. The spectral frequencies take on both positive and negative values

$$n_i \triangle k_i \equiv \frac{n_i}{N_i \triangle r_i}, \quad n_i = -\frac{N_i}{2}, \ldots, \frac{N_i}{2}. \tag{29}$$

Taking a single time step of (25) and including (26) and (27) leads to

$$\mathbf{F}\left(m_i \triangle \mathbf{r}, t\right) = \frac{1}{N_i} \sum_{n_i=0}^{N_i-1} \overline{\mathbf{A}}\left(m_i \triangle \mathbf{r}, n_i \triangle \mathbf{k_i}\right) \left\{ \sum_{p_i=0}^{N_i-1} \mathbf{F}\left(p_i \triangle \mathbf{r}, t'\right) \mathrm{e}^{-j\frac{2\pi n_i p_i}{N_i}} \right\} \mathrm{e}^{j\frac{2\pi n_i m_i}{N_i}}. \tag{30}$$

Explicit in (30) is the dependence of the state transition matrix elements on the position $\mathbf{r}$ of the field components. In an inhomogeneous space $\overline{\mathbf{A}}\left(\mathbf{r}, \mathbf{k}\right)$ is allowed to change for every $\triangle \mathbf{r}$. A complete set of spectral components exists for each state transition matrix. Computational constraints of memory and speed determine if the elements are computed once and stored or computed on the fly. The electromagnetic field propagates in the numerical space by repeated applications of (30). It is important to reiterate here that all field components are collocated in space and time.

Single Dimension Problems

This section examines the PITD method for solutions of one-dimensional problems. These problems have plane wave fields and normal incidence. Numerical concerns about stability, numerical dispersion, and numerical error are addressed and an explicit form is introduced. Maxwell's equations for a single dimension lossless region are

$$\frac{\partial H_y}{\partial x} = \varepsilon \frac{\partial E_z}{\partial t} \tag{31}$$

$$\frac{\partial E_z}{\partial x} = \mu \frac{\partial H_y}{\partial t} \tag{32}$$

where the material parameters are scalars and allowed to be functions of position x. The field components are selected and labeled to be consistent with the three-dimensional derivation. The x-

axis is the direction of propagation, the electric and magnetic field intensities are perpendicular to this direction and each other. Additionally, $k_x \equiv k$, the free space propagation constant, but the subscript will be retained. As before, rearrange (31) and (32) into a vector equation,

$$\frac{\partial}{\partial t}\begin{bmatrix} E_z \\ H_y \end{bmatrix} = \begin{bmatrix} 0 & \frac{1}{\varepsilon}\frac{\partial}{\partial x} \\ \frac{1}{\mu}\frac{\partial}{\partial x} & 0 \end{bmatrix} \cdot \begin{bmatrix} E_z \\ H_y \end{bmatrix}. \tag{33}$$

The $\mathbf{S}(x,k_x)$ matrix is a 2 x 2, which using (13) and showing the positional dependency explicitly is

$$\overline{\mathbf{S}}(x,k_x) = \begin{bmatrix} 0 & \frac{j2\pi k_x}{\varepsilon(x)} \\ \frac{j2\pi k_x}{\mu(x)} & 0 \end{bmatrix}. \tag{34}$$

The eigenvalue method finds the eigenvalues and eigenvectors of the $\overline{\mathbf{S}}(x,k_x)$ matrix in (34). Table 1 lists the two eigenvalues and their corresponding eigenvectors.

Table 1. Eigenvalues and eigenvectors for 1-D lossless materials

	Eigenvalue	Eigenvector
1	$j2\pi k_x v_p$	$\begin{bmatrix} 1 \\ 1/\eta \end{bmatrix}$
2	$-j2\pi k_x v_p$	$\begin{bmatrix} 1 \\ -1/\eta \end{bmatrix}$

Introducing the phase velocity $v_p = 1/\sqrt{\mu\varepsilon}$ and intrinsic impedance $\eta = \sqrt{\mu/\varepsilon}$ of the medium simplifies the equations. The state transition matrix derived from the eigenvalues and eigenvectors using (16) is

$$\overline{\mathbf{A}} = \begin{bmatrix} 1 & 1 \\ 1/\eta & -1/\eta \end{bmatrix} \begin{bmatrix} \exp\left(j2\pi k_x v_p \tau\right) & 0 \\ 0 & \exp\left(-j2\pi k_x v_p \tau\right) \end{bmatrix} \frac{1}{2}\begin{bmatrix} 1 & \eta \\ 1 & -\eta \end{bmatrix} \tag{35}$$

$$\overline{\mathbf{A}} = \begin{bmatrix} \cos\left(2\pi k_x v_p \tau\right) & j\eta \sin\left(2\pi k_x v_p \tau\right) \\ (j/\eta)\sin\left(2\pi k_x v_p \tau\right) & \cos\left(2\pi k_x v_p \tau\right) \end{bmatrix}. \tag{36}$$

Equation (36) is also called a rotation matrix (Nevels, *et al.* [7]) where the rotation angle is $\phi = 2\pi k_x v_p \tau$. The simplicity of this state transition matrix is exploited obtaining the explicit form of the PITD method in a later section. Equation (23), which represents a single time step or evolution of the fields, becomes

$$\begin{bmatrix} E_z(x,t) \\ H_y(x,t) \end{bmatrix} = \mathfrak{F}^{-1}\left\{ \begin{bmatrix} \cos(2\pi k_x v_p \tau) & j\eta \sin(2\pi k_x v_p \tau) \\ (j/\eta)\sin(2\pi k_x v_p \tau) & \cos(2\pi k_x v_p \tau) \end{bmatrix} \mathfrak{F}\left\{ \begin{bmatrix} E_z(x,t') \\ H_y(x,t') \end{bmatrix} \right\} \right\}. \quad (37)$$

Letting a Fourier transformed quantity be represented by a tilde over the quantity, (37) is

$$\begin{bmatrix} E_z(x,t) \\ H_y(x,t) \end{bmatrix} = \mathfrak{F}^{-1}\left\{ \begin{bmatrix} \cos(2\pi k_x v_p \tau)\tilde{E}_z(k_x,t') + j\eta \sin(2\pi k_x v_p \tau)\tilde{H}_y(k_x,t') \\ (j/\eta)\sin(2\pi k_x v_p \tau)\tilde{E}_z(k_x,t') + \cos(2\pi k_x v_p \tau)\tilde{H}_y(k_x,t') \end{bmatrix} \right\}. \quad (38)$$

Numerically equation (38) becomes

$$\begin{aligned} E_z(m\Delta x,t) &= \frac{1}{N}\sum_{n=0}^{N-1}\left(\cos(u)\tilde{E}_z(n\Delta k_x,t') + j\eta\sin(u)\tilde{H}_y(n\Delta k_x,t')\right)e^{j\frac{2\pi nm}{N}} \\ H_y(m\Delta x,t) &= \frac{1}{N}\sum_{n=0}^{N-1}\left((j/\eta)\sin(u)\tilde{E}_z(n\Delta k_x,t') + \cos(u)\tilde{H}_y(n\Delta k_x,t')\right)e^{j\frac{2\pi nm}{N}} \end{aligned} \quad (39)$$

where $u = 2\pi n \Delta k_x v_p \tau$.

Reflection from a Half Space

The geometry for the first example, reflection from a dielectric half space is in Figure 1. Standard Fourier transforms require a uniform discretization of the numerical space. The discretization chosen should provide at least two samples per wavelength in the dielectric region at the highest frequency of interest. The boundary between the two half spaces *is not* a sample point.

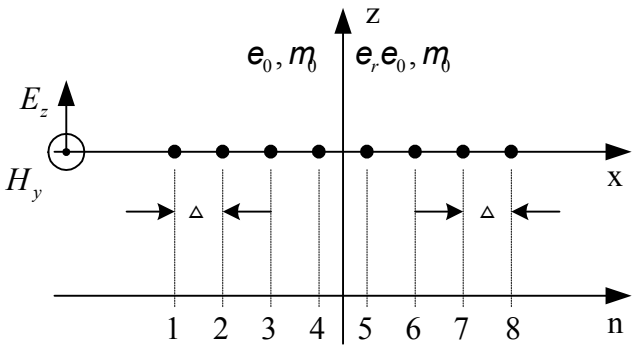

Figure 1. Reflection from a half space

The input source is a bandwidth limited Gaussian created at time zero by

$$E_z(n\Delta, t=0) = e^{-\left(\frac{n-pk}{\beta}\right)^2}, n \in \text{ free space region} \quad (40)$$

where pk is the peak location of the Gaussian and β determines the bandwidth of the signal. The maximum input electric field is one volt per meter. Because the field components are collocated in both space and time, the magnetic field is simply the electric field divided by the intrinsic impedance.

Once the initial plane wave is placed in the numerical space the path integral is evaluated by:

1. Spatially Fourier transforming the field components $\mathbf{E_z}$, $\mathbf{H_y}$.
2. Inverse Fourier transforming the product of the state transition matrix and the data from step 1. Note that for two different material regions two state transition matrices exist and the correct one for each spatial point applies to (39).

$$E_z(m,t) = \frac{1}{N}\sum_{n=0}^{N-1}\left(\cos(u)\,\tilde{E}_z(n,t') + j\eta\sin(u)\,\tilde{H}_y(n,t')\right)e^{j\frac{2\pi nm}{N}} \tag{41}$$

$$H_y(m,t) = \frac{1}{N}\sum_{n=0}^{N-1}\left((j/\eta)\sin(u)\,\tilde{E}_z(n,t') + \cos(u)\,\tilde{H}_y(n,t')\right)e^{j\frac{2\pi nm}{N}} \tag{42}$$

Table 2. State transition matrices elements

	Region	
	Free Space	Dielectric
u	$2\pi n \triangle k_x c\tau$	$2\pi n \triangle k_x \left(c/\sqrt{\varepsilon_r}\right)\tau$
u when $\tau = \triangle/c$	$2\pi n/N$	$2\pi n/N\sqrt{\varepsilon_r}$

(41) and (42) the argument of the sinusoids depends on the region (see Table 2). The distance the field propagates in a single time step is a function of the time step (τ) and the phase velocity (v_p). In a homogeneous space, one has great flexibility in choosing the time step. The natural time step $(\tau = \triangle/v_p)$ appears to be the best choice for an inhomogeneous space. For the example from Figure 1, the phase velocity chosen to calculate the time step is the speed of light in free space.

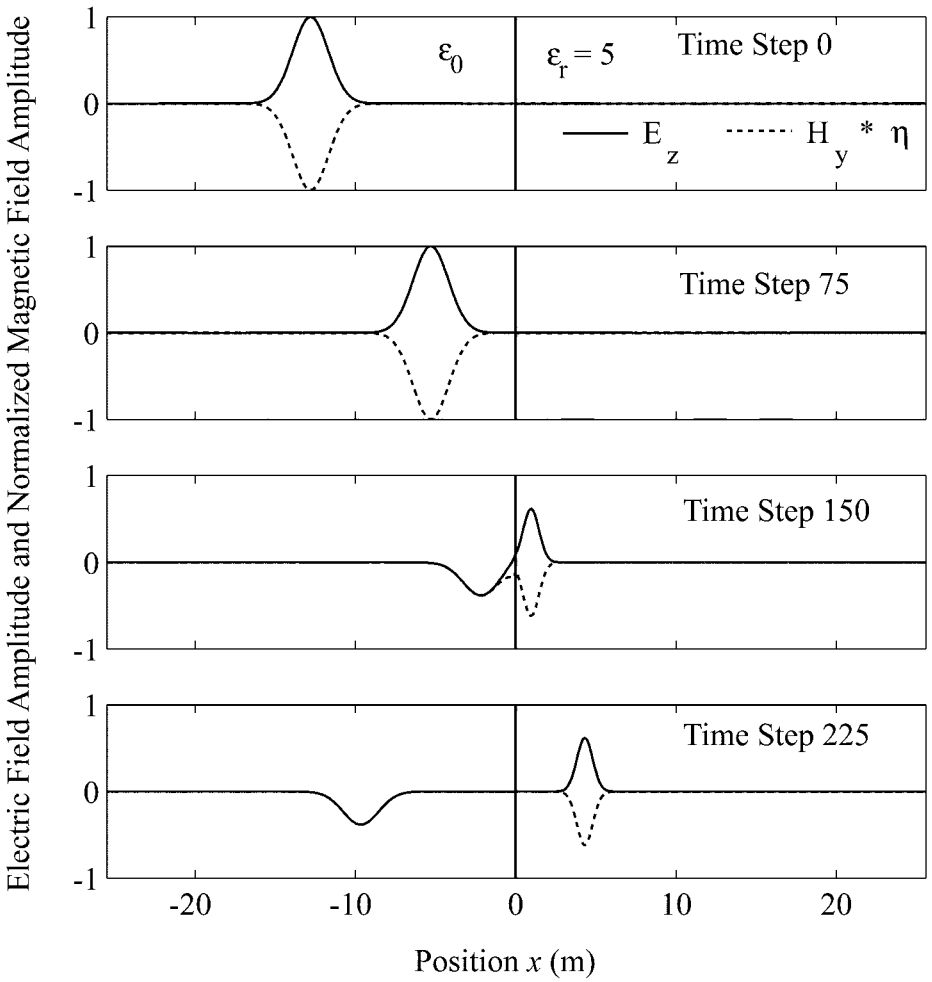

Figure 2. Reflection and transmission for a dielectric half space

Figure 2 is a series of time slices for a plane wave interacting with a dielectric half space. The intrinsic impedance in each region multiplies the magnetic field component to normalize it for display purposes. The numerical parameters for the simulation are in Table 3. The reflection coefficient is -0.382 and the transmission coefficient is 0.618. At time step 225, the forward traveling wave has a maximum electric field of $0.619\,\mathrm{V/m}$ while the scattered wave has a minimum of $-0.383\,\mathrm{V/m}$. The percent error is 0.262% and 0.162% for the reflection coefficient and transmission coefficient, respectively. Single precision computer arithmetic gave this level of accuracy.

Table 3. Reflection and transmission from a half space

N	Δ	τ	ε_r	β
512	0.1 m	Δ/c	5	$7\sqrt{\varepsilon_r}$

Kraus and Carver [8] define the energy density of a plane wave as

$$w = \frac{1}{2}\varepsilon E^2 + \frac{1}{2}\mu H^2 . \tag{43}$$

The energy density in Table 4 shows the energy density in each of the half spaces as well as the total energy. Treating the time step 0 energy density as the true value, the percent error for the total energy density is 0.173% at time steps 150 and 225. It is somewhat surprising that the energy density is slightly greater after the incident field begins interacting with the lossless dielectric half space. Fortunately, the energy density doesn't continue to increase during additional time steps. The uncertainty of the physical boundary between the two regions produces the error in the energy density.

A comparison of the magnitude of the reflection coefficient between theoretical analysis and PITD method for a half space of changing permittivity is in Figure 3. A single spatial and time discretization is kept for all permittivity values. The spatial discretization meets the Nyquist requirement of two samples per wavelength in the highest permittivity dielectric at the highest frequency contained in the Gaussian input field. The PITD method agrees to within 0.3% the theoretical value of the reflection coefficient for all permittivities.

Table 4. Energy density for scattering from a dielectric half space

Time Step	Free Space	Dielectric $\varepsilon_r = 5$	Total
0	0.1737×10^{-9}	0	0.1737×10^{-9}
75	0.1737×10^{-9}	0	0.1737×10^{-9}
150	0.0257×10^{-9}	0.1483×10^{-9}	0.1740×10^{-9}
225	0.0254×10^{-9}	0.1486×10^{-9}	0.1740×10^{-9}

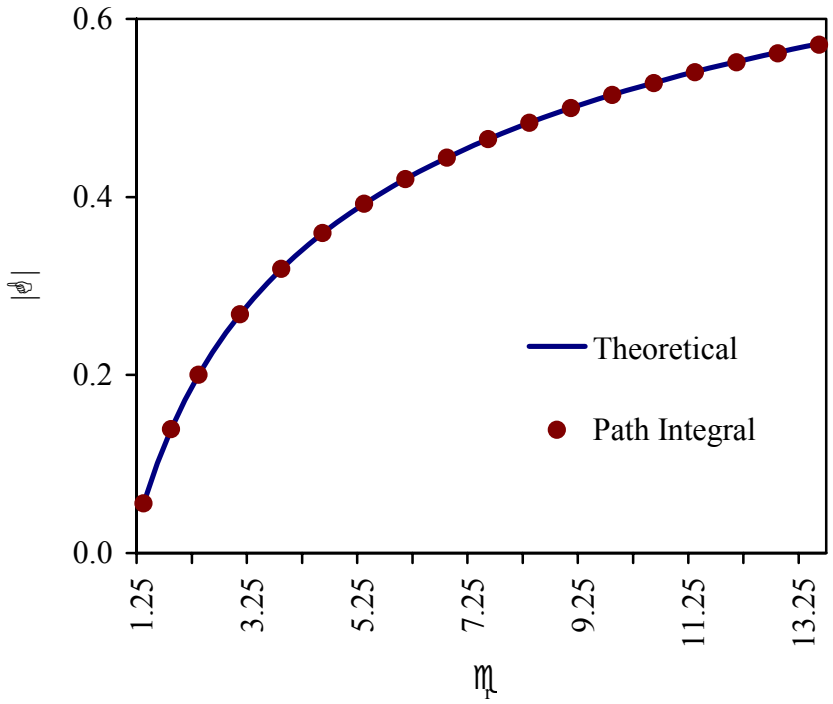

Figure 3. Absolute value of reflection coefficient from dielectric half space as a function of permittivity

Selecting the Time Step

The natural time step produces good results (Figure 2). The question remains for a problem with multiple regions as to which phase velocity to use in determining the time step. Previously the free space phase velocity determined the time step.

Figure 4 shows a set of time steps corresponding to the last pair in Figure 2 when the phase velocity of the dielectric determines the time step. Notice that the scattered field becomes jittery after reflecting from the half space. The specified time step causes the field components to traverse a single spatial step per time step inside the dielectric region. The same time step moves the field more than a single spatial amount in the free space region. The time step $\left(\tau = \Delta / c\right)$ moves the field a single spatial step per time step in the free space region while moving the field less than a spatial step per time step in the dielectric. Table 5 lists the energy density for the four time steps using the time step $\left(\tau = \Delta \sqrt{\varepsilon_r} / c\right)$. The percent error for time steps 65 and 160 are 2.99% and 2.94%, respectively.

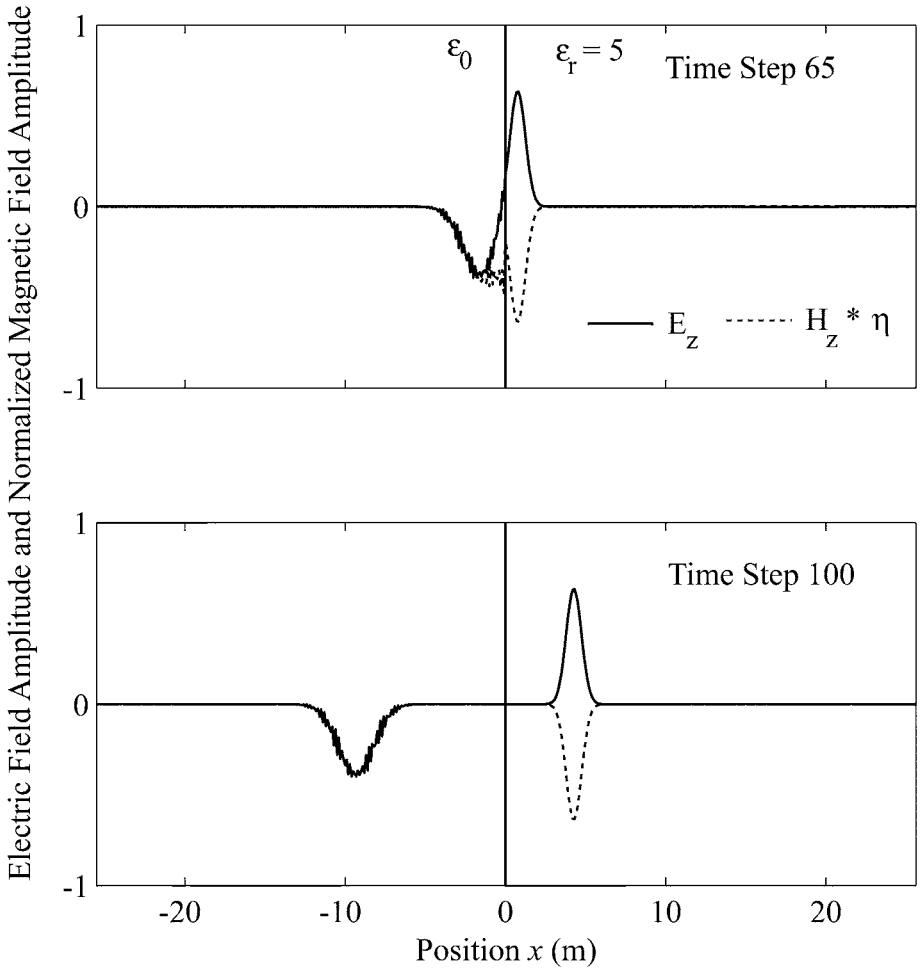

Figure 4. Reflection and transmission from a dielectric half space with natural time step in dielectric

Table 5. Energy density for a dielectric half space with natural time step in dielectric

Time Step	Free Space	Dielectric $\varepsilon_r = 5$	Total
0	0.1737×10^{-9}	0	0.1737×10^{-9}
35	0.1737×10^{-9}	0	0.1737×10^{-9}
65	0.0273×10^{-9}	0.1516×10^{-9}	0.1789×10^{-9}
100	0.0261×10^{-9}	0.1527×10^{-9}	0.1788×10^{-9}

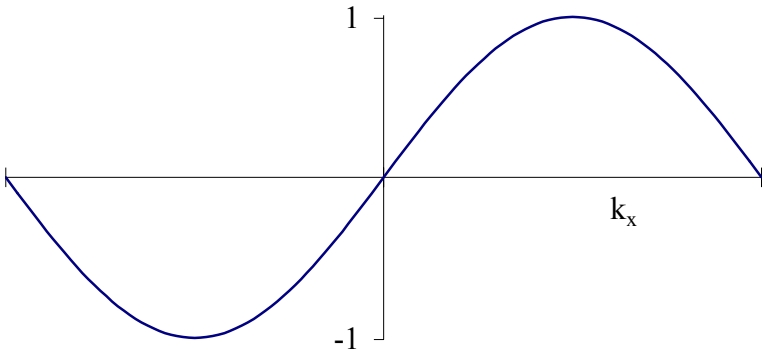

Figure 5. Natural time step with matching medium phase velocity

Carefully examining the state transition matrix elements shows how the time step relates to physical discretization. Choosing the sine term from the state transition matrix since it has a zero at the zero spatial frequency, the range for the natural time step is in Figure 5.

Figure 5 In this case, the time step is $\left(\tau = \triangle / v_p\right)$ which reduces the argument of the sinusoid to

$$u = 2\pi k_x v_p \tau = 2\pi k_x v_p \left(\triangle / v_p\right) = 2\pi k_x \triangle . \tag{44}$$

After putting equation (28) into (44) and letting n represent the discrete points, u becomes

$$u = 2\pi \left(n \triangle k_x\right) \triangle = 2\pi \left(\frac{n}{N \triangle}\right) \triangle = 2\pi \left(\frac{n}{N}\right). \tag{45}$$

Since n takes values between $-N/2$ and $N/2$, u has values between $-\pi$ and π. Therefore, the sinusoids encompass one complete cycle. Using the natural time step of free space inside a dielectric region with a greater permittivity gives an incomplete cycle as seen in

Figure 6.

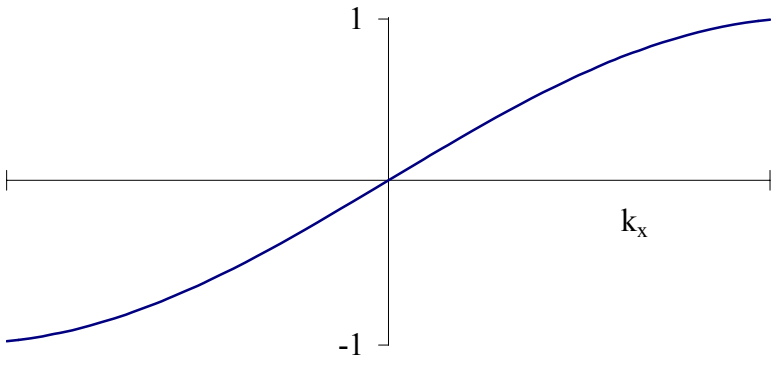

Figure 6. Different phase velocities between time step and media

This mismatch between the phase velocities of the time step and the medium gives

$$u = 2\pi k_x v_p \tau = 2\pi k_x v_p \left(\frac{\triangle}{c} \right) = 2\pi k_x \frac{c}{\sqrt{\varepsilon_r}} \frac{\triangle}{c} = 2\pi k_x \frac{\triangle}{\sqrt{\varepsilon_r}}. \tag{46}$$

Once again replacing k_x with its discrete equivalent and using (28), the argument becomes

$$u = 2\pi \left(\frac{n}{N\triangle} \right) \frac{\triangle}{\sqrt{\varepsilon_r}} = 2\pi \left(\frac{n}{N\sqrt{\varepsilon_r}} \right). \tag{47}$$

Figure 2 includes the complete and partial sinusoid ranges discussed above. In the dielectric region because of the partial cycle, the field does not propagate a spatial step per time step.

Figure 4 demonstrates the selection of the natural time step for the dielectric region. The sinusoids complete more than a cycle for the free space region, causing the field to propagate a single spatial step every time step in the dielectric but greater than a spatial step in the free space region.

Considering a homogeneous space, there are three possible choices for the time increment.

First, the natural time step provides the correct slice of time allowing the field to move a single spatial step.

Second a partial time step allowing the field to traverse a portion of the spatial step.

Third a super time step allowing the field to traverse a distance greater than a spatial step.

In a homogeneous space, any one of these time steps is valid. Figure 7 demonstrates three different time steps propagating an identical Gaussian pulse in a homogeneous space. The three time steps are: natural time step $\left(\tau = \triangle / v_p\right)$, twice the natural time step $\left(\tau = 2\triangle / v_p\right)$, and half the natural time step $\left(\tau = \triangle / 2v_p\right)$. The first time slice is the initial pulse. The second and third graphs are at time step 130. The last graph is a representation of the difference between the pulses calculated by matching the peaks of each pulse. D1 is the difference between the natural time step and twice the natural time step. D2 is the difference between the natural time step and half the natural time step. In both cases, the difference is at machine precision.

In an inhomogeneous space, the data above promotes two guidelines for selecting the spatial and temporal discretization. Calculate the natural time step using the fastest phase velocity (lowest relative permittivity and permeability). This ensures that at most a single spatial step is covered per time step in any region. The slowest phase velocity region determines the physical discretization based on highest frequency and Nyquist limit.

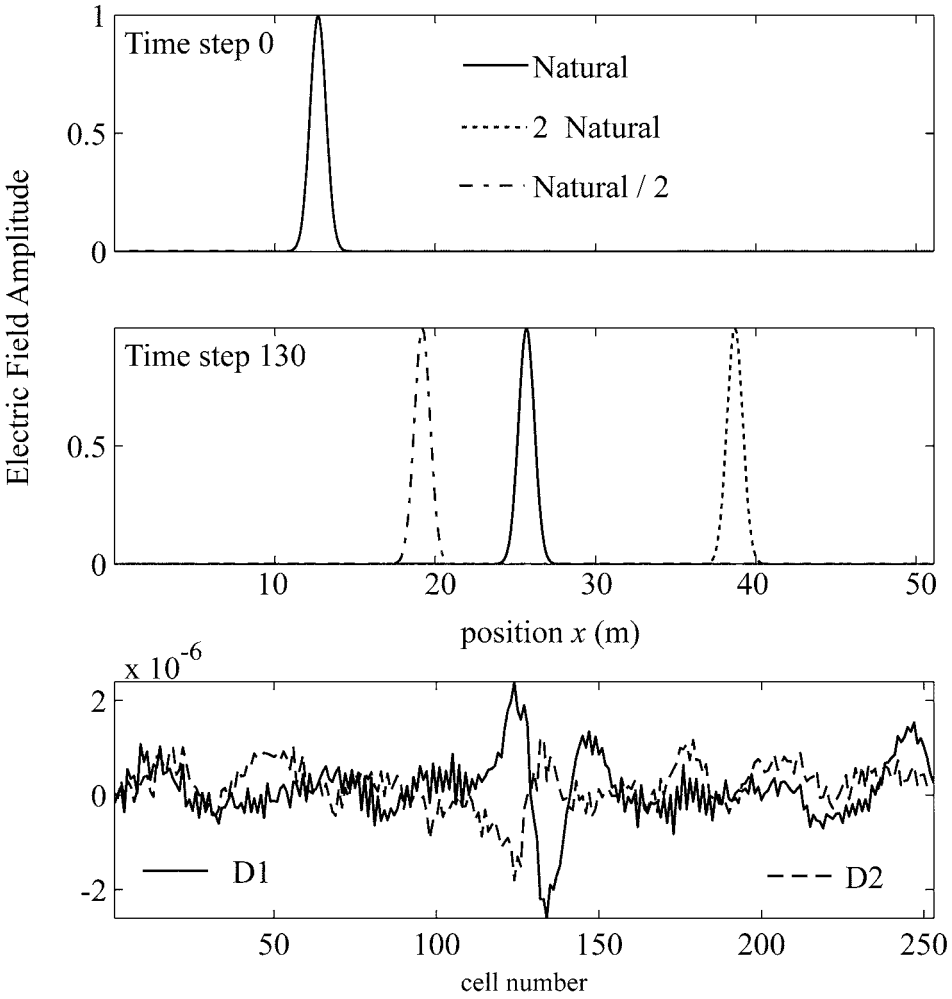

Figure 7. Time step comparison for homogeneous space

Propagation at the Nyquist Limit

The Nyquist limit is a limit numerical techniques strive to achieve. The fewer samples per wavelength a method requires translates into smaller numerical problem sizes and faster run times. The PITD method achieves propagation at the Nyquist limit in homogeneous space, as shown in Figure 8. The sample size is 0.5 meter with a time step of $\Delta/2c$ in a free space homogeneous region. The theoretical curve of a Gaussian ramped sinusoid contains many more points than the two points per wavelength of the PITD simulation. The data shows the results after propagating 1000 time steps or 500 spatial points. Propagation at the Nyquist limit is a very exciting aspect of the PITD method. When considering inhomogeneous space, the limit would apply to the slowest phase velocity material

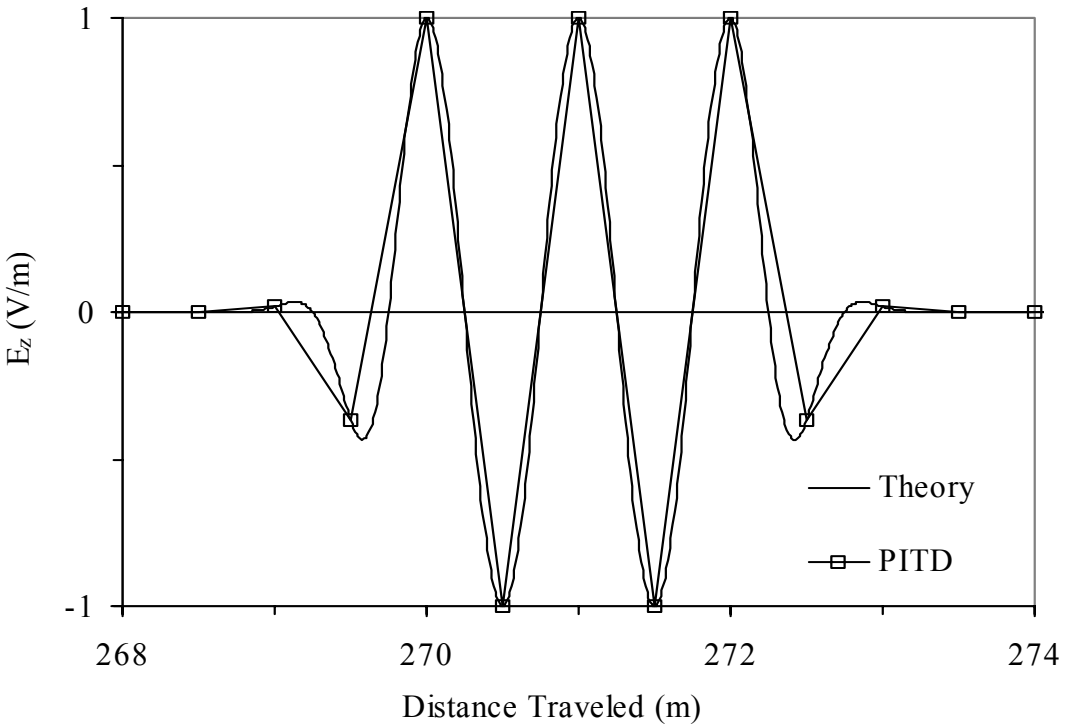

.

Figure 8. Nyquist limit propagation in one dimension

Explicit Form

Careful examination of (37) shows the inverse Fourier transform of the product of two objects. Instead of multiplying these objects in the spectral domain, equivalently, one may convolve them in the space domain giving

$$\begin{bmatrix} E_z(x,t) \\ H_y(x,t) \end{bmatrix} = \int_{-\infty}^{\infty} \mathfrak{F}^{-1}\left\{ \begin{bmatrix} \cos(u) & j\eta\sin(u) \\ (j/\eta)\sin(u) & \cos(u) \end{bmatrix} \right\} \begin{bmatrix} E_z(x-\lambda,t') \\ H_y(x-\lambda,t') \end{bmatrix} d\lambda \qquad (48)$$

with $u = 2\pi k_x v_p \tau$. The inverse spatial Fourier transform of the state transition matrix is

$$\frac{1}{2}\begin{bmatrix} \delta(\lambda - v_p\tau) + \delta(\lambda + v_p\tau) & -\eta\left(\delta(\lambda - v_p\tau) - \delta(\lambda + v_p\tau)\right) \\ -\left(\delta(\lambda - v_p\tau) - \delta(\lambda + v_p\tau)\right)/\eta & \delta(\lambda - v_p\tau) + \delta(\lambda + v_p\tau) \end{bmatrix}. \qquad (49)$$

Performing the convolution, (48) becomes

$$\begin{bmatrix} E_z(x,t) \\ H_y(x,t) \end{bmatrix} = \frac{1}{2}\begin{bmatrix} \begin{pmatrix} E_z(x - v_p\tau, t') + E_z(x + v_p\tau, t') \\ -\eta\left(H_y(x - v_p\tau, t') - H_y(x + v_p\tau, t')\right) \end{pmatrix} \\ \begin{pmatrix} -\left(E_z(x - v_p\tau, t') - E_z(x + v_p\tau, t')\right)/\eta \\ +H_y(x - v_p\tau, t') + H_y(x + v_p\tau, t') \end{pmatrix} \end{bmatrix}. \qquad (50)$$

Equation (50) shows that the current electric field is the average of the previous electric field from both sides and the difference of the magnetic field multiplied by the impedance. The locations from which the previous time data is taken match the phase velocity time step product. Notice that the electromagnetic field is not split into left and right traveling wave, but that the total field for each term on the right hand side of (50) gives the current total field. This is easily transferred into the discrete equations by replacing τ with the natural time step Δ/v_p giving

$$\begin{bmatrix} E_z(m\Delta,t) \\ H_y(m\Delta,t) \end{bmatrix} = \frac{1}{2}\begin{bmatrix} \begin{pmatrix} E_z\left((m-1)\Delta,t'\right)+E_z\left((m+1)\Delta,t'\right) \\ +\eta\left(H_y\left((m+1)\Delta,t'\right)-H_y\left((m-1)\Delta,t'\right)\right) \end{pmatrix} \\ \begin{pmatrix} \left(E_z\left((m+1)\Delta,t'\right)-E_z\left((m-1)\Delta,t'\right)\right)/\eta \\ +H_y\left((m-1)\Delta,t'\right)+H_y\left((m+1)\Delta,t'\right) \end{pmatrix} \end{bmatrix}. \tag{51}$$

In (51), the impedance on the right hand side is determined by the location of the left hand field point. The implicit form of the PITD method (performing the Fourier transforms) requires a regular spatial discretization and temporal discretization assuming standard transforming techniques are used. As previously discussed, this regular griding may result in the field being interpolated between sampling points. For the explicit form (no Fourier transforms), the same time step is kept for all regions. This allows the spatial sampling to change dependent upon the phase velocity. Once again, the actual interface between the two regions is not a sample point. The interface occurs between two of the data points.

Figure 9 shows the same four time steps as the first example.

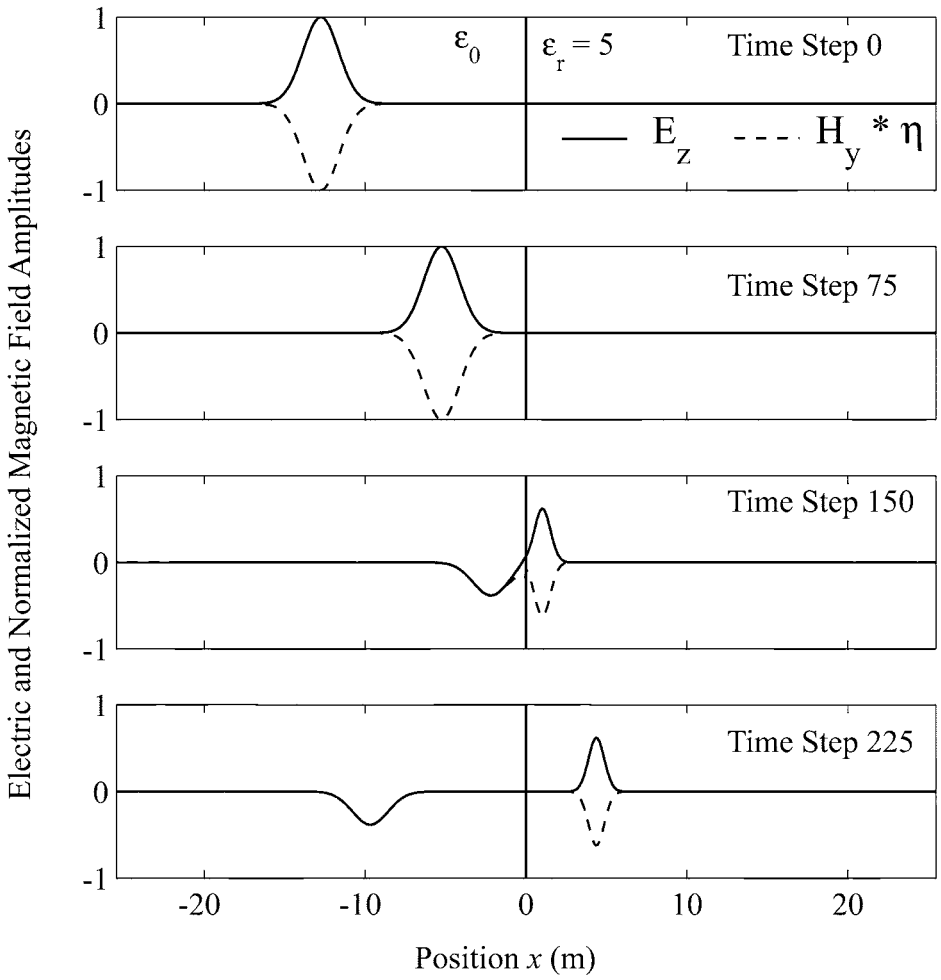

Figure 9. Explicit form showing reflection and transmission for a dielectric half space

The numerical parameters for the explicit form are similar to those in Table 3 with the difference being the spatial discretization in the dielectric region. The spatial sampling in the dielectric region is $\Delta/\sqrt{\varepsilon_r}$. The number of samples in the dielectric region was increased from 256 to 570 giving the same physical space. The reflection and transmission coefficients along with percent error are in Table 6. The reflection coefficient is slightly more accurate using the explicit form.

Table 6. Reflection and transmission coefficient for explicit form

Time Step	Reflection Coefficient	Percent Error	Transmission Coefficient	Percent Error
150	-.3822	0.052 %	.6191	0.162 %
225	-.3826	0.157 %	.6191	0.162 %

The energy density for the explicit form matched those of the implicit form in Table 4. The explicit form is a promising area of research for the PITD method.

Lossy Materials

Maxwell's equations in matrix form for a general lossy isotropic region are

$$\frac{\partial}{\partial t}\begin{bmatrix} E_z \\ H_y \end{bmatrix} = \begin{bmatrix} \dfrac{-\sigma}{\varepsilon} & \dfrac{1}{\varepsilon}\dfrac{\partial}{\partial x} \\ \dfrac{1}{\mu}\dfrac{\partial}{\partial x} & \dfrac{-\rho}{\mu} \end{bmatrix}\begin{bmatrix} E_z \\ H_y \end{bmatrix}. \tag{52}$$

The $\overline{\mathbf{S}}(x,k_x)$ matrix including (13) is

$$\overline{\mathbf{S}}(x,k_x) = \begin{bmatrix} -\dfrac{\sigma}{\varepsilon} & \dfrac{j2\pi k_x}{\varepsilon} \\ -\dfrac{j2\pi k_x}{\mu} & -\dfrac{\rho}{\mu} \end{bmatrix}. \tag{53}$$

In (53), the material parameters $(\varepsilon,\mu,\sigma,\rho)$ are functions of position and $k \equiv k_x$. The eigenvalues and eigenvectors of $\overline{\mathbf{S}}(x,k_x)$ are in Table 7.

Table 7. Eigenvalues and eigenvectors for 1-D lossy problems

	Eigenvalue	Eigenvector
1	$\dfrac{-1}{2}\left(\dfrac{\sigma}{\varepsilon}+\dfrac{\rho}{\mu}-\zeta\right)$	$\begin{bmatrix} \dfrac{j\mu}{4\pi k_x}\left\{\dfrac{-\sigma}{\varepsilon}+\dfrac{\rho}{\mu}+\zeta\right\} \\ 1 \end{bmatrix}$
2	$\dfrac{-1}{2}\left(\dfrac{\sigma}{\varepsilon}+\dfrac{\rho}{\mu}+\zeta\right)$	$\begin{bmatrix} \dfrac{j\mu}{4\pi k_x}\left\{\dfrac{-\sigma}{\varepsilon}+\dfrac{\rho}{\mu}-\zeta\right\} \\ 1 \end{bmatrix}$
Note: $\zeta = \sqrt{\left(\dfrac{-\sigma}{\varepsilon}+\dfrac{\rho}{\mu}\right)^2 - \left(4\pi k_x v_p\right)^2}$		

Putting the eigenvalues and eigenvectors from Table 7 into (16) generates the state transition matrix

$$\overline{\mathbf{A}} = \begin{bmatrix} a_{11} & a_{12} \\ a_{21} & a_{22} \end{bmatrix} \tag{54}$$

with

$$a_{11} = \left\{\cosh\left(\frac{1}{2}\zeta\tau\right) + \frac{\dfrac{-\sigma}{\varepsilon}+\dfrac{\rho}{\mu}}{\zeta}\sinh\left(\frac{1}{2}\zeta\tau\right)\right\} e^{\frac{-1}{2}\left(\frac{\sigma}{\varepsilon}+\frac{\rho}{\mu}\right)\tau}, \tag{55}$$

$$a_{12} = \frac{j4\pi k_x}{\varepsilon\zeta}\sinh\left(\frac{1}{2}\zeta\tau\right)e^{\frac{-1}{2}\left(\frac{\sigma}{\varepsilon}+\frac{\rho}{\mu}\right)\tau}, \tag{56}$$

$$a_{21} = \frac{j4\pi k_x}{\mu\zeta}\sinh\left(\frac{1}{2}\zeta\tau\right)e^{\frac{-1}{2}\left(\frac{\sigma}{\varepsilon}+\frac{\rho}{\mu}\right)\tau}, \tag{57}$$

and

$$a_{22} = \left\{\cosh\left(\frac{1}{2}\zeta\tau\right) + \frac{\frac{\sigma}{\varepsilon}-\frac{\rho}{\mu}}{\zeta}\sinh\left(\frac{1}{2}\zeta\tau\right)\right\}e^{\frac{-1}{2}\left(\frac{\sigma}{\varepsilon}+\frac{\rho}{\mu}\right)\tau}. \tag{58}$$

ζ (defined in Table 7) reduces (55)-(58) to a manageable size. Letting both the conductivity (σ) and resistivity (ρ) go to zero returns the lossless state transition matrix. Selecting the geometry in Figure 1 but replacing the dielectric region with a lossy dielectric specified in Table 8 provides the results in Figure 10. The reflection coefficient is -0.382 which agrees with the theoretical result.

Table 8. General lossy one-dimensional data parameters

N	Δ	τ	ε_r	μ_r	σ	ρ	β
512	0.1 m	Δ/c	5	1	1.328×10^{-4}	3.7699	$7\sqrt{\varepsilon_r}$

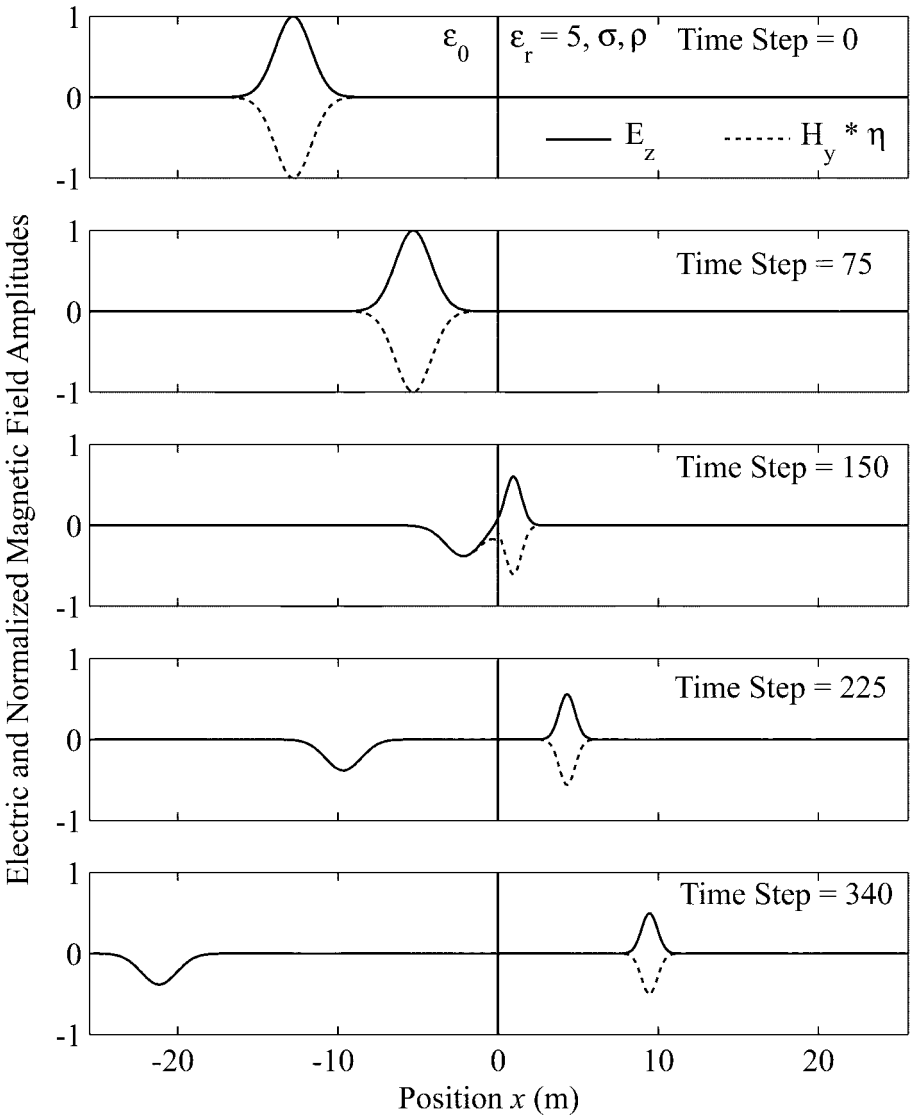

Figure 10. Reflection and transmission from a general lossy half space

Absorbing Boundary Conditions

There are two very effective absorbing boundary conditions (ABC) for the one dimensional PITD method. The first boundary condition is a perfectly matched layer (PML). Berenger [9] extended planar absorbing layers to non-normal incidence, which is an important consideration for higher dimensional spaces. The second boundary condition appears to be unique to the PITD method. It is termed the null boundary (NB) and is the simplest boundary condition to implement. Single dimensional spaces provide a decided advantage when considering ABCs. The field is always normal to the boundary so there is no concern about angle dependence of the reflection coefficient. PML is a series of layers with progressively higher loss but constant impedance. This absorbs the incident wave without reflection. The reflection coefficient (Γ) is calculated from the intrinsic impedances by

$$\Gamma = \frac{\eta_2 - \eta_1}{\eta_2 + \eta_1} \tag{59}$$

where the subscript indicates the region and the field is incident from region 1 into region 2. Obviously, if $\eta_2 = \eta_1$ there is no reflection. In the frequency domain, the intrinsic impedance is a complex value that is frequency and loss (σ, ρ) dependent. For the time-domain, it is essential that the reflection coefficient be constant for all frequencies and zero. Therefore, a relationship between $\varepsilon, \mu, \sigma,$ and ρ is needed. Starting with

$$\zeta = \sqrt{\left(\frac{-\sigma}{\varepsilon} + \frac{\rho}{\mu}\right)^2 - \left(4\pi k_x v_p\right)^2} \tag{60}$$

and letting

$$\frac{\sigma}{\varepsilon} = \frac{\rho}{\mu} \tag{61}$$

then

$$\begin{aligned} \zeta &= \sqrt{(0)^2 - \left(4\pi k_x v_p\right)^2} \\ \zeta &= j4\pi k_x v_p \end{aligned} \tag{62}$$

resulting in

$$\overline{\mathbf{A}} = \begin{bmatrix} \cosh\left(j2\pi k_x v_p \tau\right) & \eta \sinh\left(j2\pi k_x v_p \tau\right) \\ \sinh\left(j2\pi k_x v_p \tau\right)/\eta & \cosh\left(j2\pi k_x v_p \tau\right) \end{bmatrix} \mathrm{e}^{\frac{-\sigma}{\varepsilon}\tau}. \tag{63}$$

The hyperbolic trigonometric functions of complex argument reduces to normal trigonometric functions of real argument resulting in

$$\overline{\mathbf{A}} = \begin{bmatrix} \cos\left(2\pi k_x v_p \tau\right) & j\eta \sin\left(2\pi k_x v_p \tau\right) \\ j\sin\left(2\pi k_x v_p \tau\right)/\eta & \cos\left(2\pi k_x v_p \tau\right) \end{bmatrix} \mathrm{e}^{\frac{-\sigma}{\varepsilon}\tau}. \tag{64}$$

Notice equation (64) is the lossless state transition matrix with a multiplication by a loss term. Selecting equation (61) ensures that the impedance is constant in each layer for all frequencies and the loss is a simple exponential multiplier. Following the work of Berenger [9], a nine cell ABC with each layers σ_i a parabolic function of depth defined by

$$\sigma_i = \frac{\sigma_m}{\delta^2}\left((i\triangle)^2 + (\triangle)^2/12\right) \tag{65}$$

where $\delta = 9\triangle$ is the width of the absorbing zone (nine cells) and

$$\sigma_m = \frac{3\varepsilon v_p \left|\ln R\right|}{2\delta} \tag{66}$$

with $R = 10^{-5}$. Though PML performance is not demonstrated here, previous works have demonstrated reflectionless performance on the order of machine error.

The null boundary (NB) is one of those accidents of science. It was discovered while examining perfect electric conductors (PEC) in the PITD method. Since the electric and magnetic fields are zero inside a PEC, the field components for sample points inside the conductor are zeroed. When the program ran, the field did not reflect from this "PEC" but instead were absorbed by it. The reason becomes apparent by looking closely at the explicit form (51). Concentrating on the electric field component

$$E_z\left(m\vartriangle,t\right)=\frac{1}{2}\begin{pmatrix}E_z\left(\left(m-1\right)\vartriangle,t'\right)+E_z\left(\left(m+1\right)\vartriangle,t'\right)\\+\eta\left(H_y\left(\left(m-1\right)\vartriangle,t'\right)-H_y\left(\left(m+1\right)\vartriangle,t'\right)\right)\end{pmatrix}, \tag{67}$$

the current time electric field at location m is the average of the electric field on either side plus the half of the difference of the magnetic field multiplied by the impedance at m. Now assume that the "PEC" is to the right of m, the field is always zero and (67) reduces to

$$E_z\left(m\vartriangle,t\right)=\frac{1}{2}\left(E_z\left(\left(m-1\right)\vartriangle,t'\right)+\eta H_y\left(\left(m-1\right)\vartriangle,t'\right)\right). \tag{68}$$

A field $E_z\left(m,t\right)$ at the boundary is therefore only computed from the field to the left of the boundary. No reflection occurs, because the field at the boundary can only travel into the boundary. Equation (68) is also the equation obtained for the leading point of a plane wave traveling in space. Having discovered this ABC by accident, a question remains concerning its effectiveness. The boundary is actually a single cell on either end of the space.

Table 9. One-dimensional ABC numerical parameters

N	$\vartriangle$	τ	ε_r	μ_r	β	PML	NB
512	0.1 m	$\vartriangle/c$	1	1	$7\sqrt{\varepsilon_r}$	9 cell ABC	1 cell ABC

The null boundary condition has consistently demonstrated equivalent performance to the PML absorbing boundary within machine precision.

Conclusion

The PITD method is a numerical technique still in its infancy. It has several intriguing properties as well as straightforward physical discretization. No sample point lies on a physical boundary between inhomogeneous spaces. This avoids complicating the method development or the 'ordering problem' of needing to apply the differential operators in $\overline{\mathbf{S}}$ to both the material parameters and the field.

The PITD method is stable and a unitary operation. In a homogeneous space, the only numerical error derives from the finite precision math of the computer and the Fourier transform. This indicates that the PITD method is accurate to the machine precision. The small error found in reflection and transmission through a half space are linked to the inexact location of the interface. The PITD method requires sampling at the Nyquist limit, which is two samples per wavelength at

the highest frequency of interest. This is a very significant factor since most numerical techniques require sampling much finer than the Nyquist limit. The explicit form does not require any numerical Fourier transforms. The PITD method does not suffer from numerical dispersion.

The time step choice is important for inhomogeneous spaces but open for homogeneous space. The natural time step for a homogeneous space moves the field one spatial step every time step. In an inhomogeneous space, the problem time step should match the natural time step for the fastest phase velocity region of the problem. This choice ensures that the field will not travel more than a spatial step per time step in any regions. The spatial discretization is determined by the Nyquist limit for the highest frequency of interest in the slowest phase velocity region. The range of the sinusoids in the lossless state transition matrix has a simple relationship determining the field's spatial movement. A complete cycle moves the field a spatial step per time step, less or more than a cycle moves the fields less or more than one spatial step.

Two ABCs show excellent effectiveness in terminating the numerical space. The PML implemented with several layers of lossy material. Fortunately, the loss term is a separate exponential that does not increase the computational cost significantly. The number of layers and the loss profile are both active research areas for other methods as well as this one. The null boundary requires a single cell for application and is computationally effortless.

Recently, Nevels and Jeong [10] reported an explicit form for a general one-dimensional lossy material. This has wide application in transmission line studies. At its current state of development, the PID method is well suited for one-dimensional problems. It is especially straightforward in illustrations for pedagogical purposes.

REFERENCES

[1] R. Nevels, J. Miller, and R. Miller, "A path integral time-domain method for electromagnetic scattering," *IEEE Trans. Antennas Propagat.,* vol. AP-48, no. 4, pp. 565-573, April 2000.

[2] G. Barton, *Elements of Green's Functions and Propagation: Potentials, Diffusion, and Waves*, New York: Oxford University Press, 1995.

[3] P. DeRusso, R. Roy, and C. Close, *State Variables for Engineers,* New York: John Wiley & Sons, 1965.

[4] D. M. Wiberg, *Schaum's Outline of Theory and Problems of State Space and Linear Systems,* New York: McGraw-Hill, 1971.

[5] R. Ziemer, W. Tranter, and D. Fannin, *Signals and Systems: Continuous and Discrete,* New York: Macmillan Publishing Co., 1983.

[6] W. Press, S. Teukolsky, W. Vetterling, and B. Flannery, *Numerical Recipes in C: The Art of Scientific Computing,* Cambridge: Cambridge University Press, 1992.

[7] R. Nevels, J. Miller, and R. Miller, "Rotation in Electromagnetic Field Equations: A Discussion, Interpretation and Application," *Digest of the 1998 IEEE AP-S/URSI International Symposium*, Atlanta, Georgia, June 1998, pp. 875-878.

[8] J. D. Kraus and K. R. Carver, *Electromagnetics,* Tokyo: McGraw-Hill Kogajusha, 1981.

[9] J.-P. Berenger, A perfectly matched layer for the absorption of electromagnetic waves, *J. Computational Physics*, vol. 114, no. 2, pp. 185-200, Oct. 1994.

[10] R. D. Nevels and J. Jeong, "The electromagnetic field in a 1-D lossy medium based on a maxwell equation propagator," *Digest of the 2004 IEEE AP-S/URSI International Symposium*, Monterey, California, June 2004, pp. 2055-2058.